Comparison of Methods to Estimate Snow Water Equivalent at the Mountain Range Scale: A Case Study of the California Sierra Nevada

MELISSA L. WRZESIEN AND MICHAEL T. DURAND

School of Earth Sciences, and Byrd Polar and Climate Research Center, The Ohio State University, Columbus, Ohio

TAMLIN M. PAVELSKY

Department of Geological Sciences, University of North Carolina, Chapel Hill, North Carolina

IAN M. HOWAT

School of Earth Sciences, and Byrd Polar and Climate Research Center, The Ohio State University, Columbus, Ohio

STEVEN A. MARGULIS AND LAURIE S. HUNING

Department of Civil and Environmental Engineering, University of California, Los Angeles, Los Angeles, California

(Manuscript received 18 October 2016, in final form 6 January 2017)

ABSTRACT

Despite the importance of snow in global water and energy budgets, estimates of global mountain snow water equivalent (SWE) are not well constrained. Two approaches for estimating total range-wide SWE over Sierra Nevada, California, are assessed: 1) global/hemispherical models and remote sensing and models available for continental United States (CONUS) plus southern Canada (CONUS+) available to the scientific community and 2) regional climate model simulations via the Weather Research and Forecasting (WRF) Model run at 3, 9, and 27 km. As no truth dataset provides total mountain range SWE, these two approaches are compared to a ''reference'' SWE consisting of three published, independent datasets that utilize/validate against in situ SWE measurements. Model outputs are compared with the reference datasets for three water years: 2005 (high snow accumulation), 2009 (average), and 2014 (low). There is a distinctive difference between the reference/WRF datasets and the global/CONUS+ daily estimates of SWE, with the former suggesting up to an order of magnitude more snow. Results are qualitatively similar for peak SWE and 1 April SWE for all three years. Analysis of SWE time series indicates that lower SWE for global and CONUS+ datasets is likely due to precipitation, rain/snow partitioning, and ablation parameterization differences. It is found that WRF produces reasonable (within 50%) estimates of total mountain range SWE in the Sierra Nevada, while the global and CONUS+ datasets underestimate SWE.

1. Introduction

With more than 33 million km^2 of the planet's land area classified as mountains (~25% of total land area; Meybeck et al. 2001) and more than 50% of mountainous areas functioning as snow-bearing ''water towers'' for regions downstream (Viviroli et al. 2007), montane snow water equivalent (SWE) is a critical part of the global water cycle. A significant fraction of Earth's human population depends on montane snowmelt for water resources (Barnett et al. 2005). For instance, Southern California receives nearly 60% of its water from the Sierra Nevada snowpack (Waliser et al. 2011).

Despite its importance, our ability to characterize mountain snowpack globally remains poor (Lettenmaier et al. 2015; Dozier et al. 2016). Mountain environments pose challenges for collecting field data; many mountain ranges lack large-scale observational networks (Renwick 2014). Mudryk et al. (2015) recently compared available SWE estimates over the Northern Hemisphere, including global climate models, offline models, and remote sensing SWE estimates. They found that peak SWE values differ by up to 50%, with mountain regions playing a large role in these differences. Despite recent improvements, global climate model spatial resolution is too coarse to properly

Corresponding author e-mail: M. L. Wrzesien, wrzesien.1@osu.edu

DOI: 10.1175/JHM-D-16-0246.1

represent processes in areas with complex topography (IPCC 2013; Rasmussen et al. 2011). This is problematic, as mountainous regions are warming faster than the rest of the world (Pepin et al. 2015). Without baseline estimates of global mountain snowpack estimates, it will be difficult or impossible to quantify how those values may change in a future, warmer climate (IPCC 2013). It is thus urgent to improve methods for characterizing montane snow at the scale of mountain ranges. In this context, regional climate model (RCM) simulations may provide a useful tool for estimating total mountain range SWE. For example, Rasmussen et al. (2011) and Wrzesien et al. (2015) present RCM simulations for the Colorado Rocky Mountains and central Sierra Nevada, respectively; in both cases, the model successfully simulated spatial and temporal patterns of SWE.

Our objective in this study is to evaluate whether existing datasets available to the community or Weather Research and Forecasting (WRF) Model RCM simulations can produce ''reasonable'' (defined here as ±50%) estimates of total mountain range SWE. We examine this question in the California Sierra Nevada; although in situ snow measurement density is just 1 per 700 km^2 (Guan et al. 2013), it is relatively dense compared to other ranges. Several estimates of total Sierra Nevada SWE volume are available from the literature (Howat and Tulaczyk 2005; Dozier et al. 2016; Margulis et al. 2016), which is not true of many other ranges.

As there is no total mountain range SWE ''truth'' dataset, we compare to a set of ''reference'' SWE estimates that consists of three separate datasets, each of which is either based on, or validated against, in situ SWE measurements: 1) an interpolation of in situ SWE stations (Dozier et al. 2016); 2) the Sierra Nevada Snow Reanalysis (SNSR), a 90-m data assimilation of Landsat snow cover fraction data, which was extensively validated against in situ data (Margulis et al. 2016); and 3) the National Weather Service Snow Data Assimilation System (SNODAS) SWE product (Carroll et al. 2001), which is constrained to match in situ SWE. These datasets represent three very different approaches: a relatively traditional method; a new, advanced method; and an operational approach. We acknowledge and discuss scaling issues related to assuming point observations are representative of grid-scale SWE, below. However, we argue that the range of values provided by the reference datasets represents the most likely estimate of range-scale SWE for the Sierra Nevada.

We assess five globally available gridded SWE datasets derived from both models and remote sensing measurements, with resolutions ranging from 24 to 80 km, and five gridded datasets that are produced for the continental United States (CONUS) plus southern Canada (CONUS+, hereafter), with resolutions ranging from 14 to 32 km. We also produce WRF RCM simulations over the Sierra Nevada domain, at three spatial resolutions: 27, 9, and 3 km. We consider a high (2005), an average (2009), and a low (2014) accumulation year, and we compare the total range SWE (km^3) among all products. Dataset descriptions and detailed hypotheses as to their expected performance are provided below.

2. Background

Given our objectives, it is unavoidable to compare in situ observations to gridcell estimates from models and remote sensing. Thus, it is helpful to briefly review terminology and concepts related to spatial scaling in snowpack modeling. Background on previous work in snow modeling, remote sensing, and interpolation is also presented.

a. Scaling between grids and point observations of snow

Bridging the scale mismatch between the relatively coarse spatial grids used by models and point-scale in situ observations is a long-standing problem in snow hydrology (e.g., Blöschl 1999), and it is relevant here as it relates to the fidelity of the reference datasets. All of the reference datasets connect point observations and gridded SWE products, either by validating against them, assimilating them, or interpolating them; in each case, it is implicitly assumed that the in situ observation is representative of a gridded area. As there are few other alternatives, this is done regularly for both offline and online models (Leung and Qian 2003; Etchevers et al. 2004; Essery et al. 2009; Rutter et al. 2009; Rasmussen et al. 2011; Pavelsky et al. 2011; Wrzesien et al. 2015; Snauffer et al. 2016), despite the fact that such comparisons are inherently problematic (Blöschl 1999; Molotch and Bales 2005; Nolin 2012). For instance, Rasmussen et al. (2011) assume that in situ observation locations are representative of 2-km grid cells, but such a spatial scale can cross mountain crests and watershed boundaries, encompassing a range of elevations, slopes, and aspects.

Clark et al. (2011) describe four modeling scales: point scale (<5 m), hillslope scale (1–100 m), watershed scale (100–10 000 m), and regional scale (10–1000 km), and describe processes important at each scale. Blöschl (1999) defines the process scale of snow properties, the measurement scale, and the model scale. Shifting from the process scale to either the measurement scale (such as a snow course) or the model scale (such as a grid cell) affects statistical properties of each estimate, such as variance and correlation length, and can introduce bias.

Blöschl (1999) also describes the scale triplet—spacing, extent, and support. Spacing is the distance between samples or observations, which corresponds to the spacing between point snow measurements, for instance, or to model grid size. Extent is the whole area that is modeled or sampled, such as the entire model domain. Support is the area over which the estimate is averaged, such as a single model grid cell.

It is impossible to completely overcome the scale mismatch between point observations and gridded model estimates. Given the inherent problems with scaling between measurements and models, we will discuss the issues and provide appropriate caveats to our conclusions. However, we believe that gridded products that are constrained by or validated against the in situ data, as the three reference datasets are, are likely the best option for a reasonable estimate of range-wide SWE.

b. *Available methods for estimating SWE in mountain areas*

As described by Dozier et al. (2016), there are four main techniques for estimating mountain SWE: 1) interpolating in situ measurements; 2) satellite measurements, whether from passive microwave or gravity sensors; 3) reconstructing SWE from visible satellite observations and energy balance estimates; and 4) modeling SWE.

1) Interpolation of in situ observations

Operational snow courses represent a permanent location where SWE measurements are made at regular intervals along a transect; typical spatial support is tens of square meters. Snow pillows are automated weighing devices installed permanently in the landscape, with typical dimensions of 3 m × 3 m. Interpolation schemes regress snow point observations with meteorological and physiographic data and then krige the residuals; typical grid sizes are 1–3 km. Howat and Tulaczyk (2005) produced an SWE interpolation for the Sierra Nevada over a 53-yr record that captured 68% of the spatial variance, on average, in the measured SWE, with a mean error of 27%. Fassnacht et al. (2003) investigated several interpolation techniques over three water years for the Colorado River basin; the results for the best method were unbiased, with root-mean-square errors less than 155 mm.

When using an interpolated product, the assumption is that the point measurement represents the entire grid cell; for typical 1–3-km grids, processes operating at both the hillslope and watershed scales control subgrid SWE variations via controls of slope and aspect on wind redistribution and available melt energy, among other factors (Clark et al. 2011). Both snow pillows and snow courses are typically situated in relatively flat, open areas or forest clearings that are sheltered from wind. Detailed field studies have shown that snow pillows and snow courses can be nonrepresentative of the surrounding pixel sizes. Molotch and Bales (2005) show that snow telemetry sites in the Rocky Mountains can overestimate surrounding SWE by up to 200%. Nolin (2012) illustrated the failure of the in situ network to capture SWE spatial patterns, particularly in a changing climate. Meromy et al. (2013) performed 53 assessments at 15 snow pillow and snow course locations across the western United States. In contrast with previous work, across the 53 assessments, only 26 had biases greater than 10%. In summary, when utilizing interpolation to approximate range-wide SWE, bias cannot be ruled out, in part because of the fact that measured SWE is generally nonrepresentative of the pixel.

2) Satellite measurements

Global- and continental-scale SWE estimates based on microwave satellite observations exist. Global Snow Monitoring for Climate Research (GlobSnow; Takala et al. 2011) has produced a merger of microwave and in situ measurements that quantifies SWE globally, but neglects mountain snow altogether. The standard NASA passive microwave product performs poorly for deep snow and in forests, two conditions that often prevail in the mountains (Vuyovich et al. 2014); this is likely due to algorithm issues, rather than spatial scale per se (Durand et al. 2009). GRACE satellites estimate terrestrial water storage changes (Schmidt et al. 2006) based on gravity measurements. However, GRACE resolution is too coarse to deconvolve changes in mountain snowpack from other signals at the appropriate spatial resolution (e.g., Syed et al. 2008) without significant local in situ data (e.g., Famiglietti et al. 2011), which are unavailable in most global ranges.

3) Reconstructions and the SNSR

Traditional SWE reconstruction combines remote sensing observations of snow cover with an energy balance model to estimate SWE throughout the accumulation season (Cline et al. 1998; Guan et al. 2013). The SNSR (Margulis et al. 2016) is a probabilistic extension of SWE reconstruction (Girotto et al. 2014). Uncertainties in meteorological and other inputs are parameterized and prior model estimates are conditioned on independent remote sensing data to generate a posterior estimate. The result is a spatially and temporally consistent estimate at the chosen model resolution. One disadvantage of both reconstructions in general and the SNSR specifically is that they can only be performed

post facto, that is, once satellite imagery of snow ablation is available.

4) MODELING

(i) Modeling snowpack mass and energy balance

Accurate snowpack simulations must correctly model both accumulation and ablation. Accurate accumulation requires simulating the precipitation correctly, which is difficult to validate since gauge undercatch of 50% is not uncommon (Pan et al. 2003). Partitioning rain versus snow is important so the simulated precipitation falls as the correct phase (Kienzle 2008; Marks et al. 2013). Accurate temperature forcing data are crucial for determining precipitation phase and snowpack ablation rates. Longwave radiation simulation, which relies on simulation of the snow surface temperature, is critical for accurate snow ablation estimates. Snow albedo simulation is also crucial, as absorbed shortwave radiation is one of the main drivers of melt. Accurate albedo simulation is challenging, as it depends on snow grain size, impurities, and snow depth. The effects of forest cover exacerbate many of these challenges, intercepting and storing some snowfall within the canopy, dramatically modulating energy fluxes in complex ways (e.g., Lundquist et al. 2013). The Snow Model Intercomparison Project (SnowMIP; Etchevers et al. 2004) found that more complex, multilayered models generally produced more accurate SWE simulations, for example, producing less bias in outgoing longwave radiation, which is critical particularly during the accumulation season. A follow-on project, SnowMIP2, found that the effect of forest cover generally degrades model performance, with less intermodel consistency in forested areas (Rutter et al. 2009).

(ii) Offline versus coupled modeling

In an uncoupled land surface model (LSM), the land surface physics, including snow cover, evolve based on meteorological forcing data from either measurements or an atmospheric model. Therefore, there are no feedbacks between the land surface and the atmosphere. Running an uncoupled model often requires a constant lapse rate assumption (usually $6.5°C\,km^{-1}$). However, recent studies suggest seasonality in lapse rates in complex topography (Minder et al. 2010). Coupled models, on the other hand, allow for interaction between the land surface and the atmosphere. Coupling between snow and the atmosphere is the strongest during snowmelt because of the snow albedo effect on surface radiative balance (Xu and Dirmeyer 2011). In addition, a coupled RCM with high-resolution topography is more likely to provide adequate spatial precipitation patterns than is an interpolation of sparse precipitation observations required by offline modeling, because RCMs simulate airmass uplift and orographic precipitation directly (Rasmussen et al. 2011).

Dynamical downscaling offers the potential to run coupled regional models at much finer resolution than global models, enabling simulations of coupled processes at high resolution (Lo et al. 2008; Caldwell et al. 2009; Rasmussen et al. 2011). In this case, a global model or reanalysis product provides the outermost boundary conditions, but inner domains receive forcing data from the domain enclosing it. By nesting fine-resolution inner domains within coarser-resolution outer domains, grid spacing as fine as 2–4 km has been reported for seasonal-to-annual simulations over mountainous domains (Leung and Qian 2003; Done et al. 2004; Ikeda et al. 2010; Rasmussen et al. 2011; Pavelsky et al. 2011; Wrzesien et al. 2015).

3. Datasets

a. Snow courses

We use snow course measurements from the Department of Water Resources California Data Exchange Center (http://cdec.water.ca.gov) to produce the gridded interpolation product, as described in section 4. For each of the three study years, there are over 250 snow courses with 1 April SWE observations. All stations are located between 1326 and 3490 m in elevation, with an average elevation of 2371 m; 75% of the stations are located below 2717 m and there are no observations above 3490 m, though 2% of the Sierra Nevada is above 3490 m ($\sim$1200 km^2). Since the in situ network is not widespread at the high elevations, few or no observations are available for comparison or to inform the interpolation. Locations of the stations used for the water year 2009 interpolation are shown in Fig. 1.

b. Gridded datasets

Here, we describe 12 observational datasets for which we evaluate estimates of mountain range–scale SWE; they originate from eight sources, with some sources providing multiple datasets. Some datasets are available globally, while others are only provided for CONUS+ or the Sierra Nevada. While other datasets are available, they are either very coarse resolution (e.g., NCEP–NCAR reanalyses; Kalnay et al. 1996) or deliberately exclude most mountain regions (e.g., GlobSnow; Takala et al. 2011), as microwave retrievals are challenging in mountainous areas (e.g., Durand and Margulis 2007).

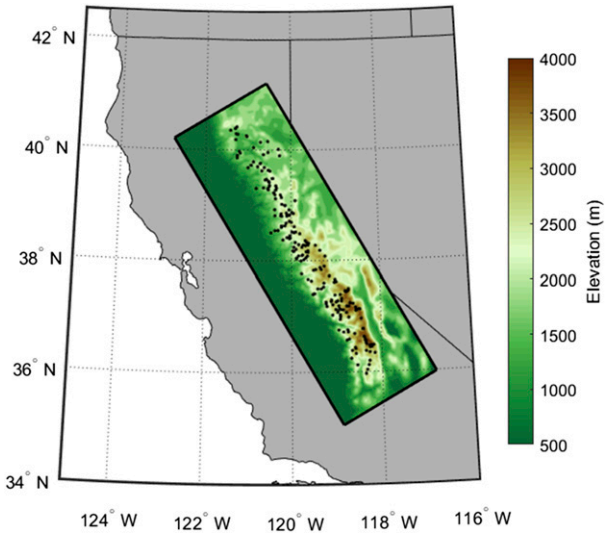

FIG. 1. Elevation, from 3-km WRF domain, over the study region of the Sierra Nevada. Black dots indicate in situ observation locations associated with snow courses.

1) AMSR-E

The Advanced Microwave Scanning Radiometer for Earth Observing System (AMSR-E) passive microwave instrument allows for a daily/near-daily, global SWE product based on brightness temperature retrievals. We use the level-3 SWE product produced for the Northern Hemisphere at 25-km resolution Equal-Area Scalable Earth Grids, which is available for download at the National Snow and Ice Data Center (NSIDC; Tedesco et al. 2004). Since there are orbit gaps in the daily product, we use the 5-day pentad to ensure a geographically complete SWE product over the study region. AMSR-E is not available for the 2014 comparison since data production stopped in 2011 because of instrument failure.

Multiple studies have evaluated the ability of the passive microwave product to estimate SWE. Tedesco and Narvekar (2010) compare AMSR-E to SNODAS across the continental United States and show that there is poor correlation between the two datasets, with a correlation coefficient R of only 0.17. They hypothesize that terrain heterogeneity within an AMSR-E pixel further reduces the correlation between the two products. Vuyovich et al. (2014) compare AMSR-E to SNODAS across the same region and show high correlations for the Great Plains (statistically significant coefficient of determination $R^2 = 0.47$–0.66) and the lower Colorado River basin (statistically significant $R^2 = 0.65$), but in densely vegetated areas and regions with deep snowpack, passive microwave SWE estimates are significantly lower than SNODAS estimates. They find the highest correlations occur where SWE accumulation is less than 200 mm and forest fraction is less than 20%. We choose to include AMSR-E in this analysis to quantify the performance at the mountain range scale.

2) GLDAS

The Global Land Data Assimilation System (GLDAS; Rodell et al. 2004) dataset produces global estimates of assimilated meteorological variables, as well as SWE. We utilize both the older GLDAS, version 1 (GLDAS-1), and the more recent GLDAS, version 2 (GLDAS-2), products (GLDASv1 and GLDASv2, respectively, hereafter), both of which have a resolution of 0.25° (~28 km) and are from the Goddard Earth Sciences Data and Information Services Center (GES DISC; http://disc.sci.gsfc.nasa.gov/hydrology/data-holdings). For our three study years, GLDASv1 forcing data are from the National Oceanic and Atmospheric Administration (NOAA) Global Data Assimilation System atmospheric analysis fields, NOAA Climate Prediction Center (CPC) Merged Analysis of Precipitation fields, and the Air Force Weather Agency's Agricultural Meteorological modeling system's downward shortwave and longwave radiation fields. Over the entire period that GLDASv2 is available, it is forced with the Global Meteorological Forcing Dataset from Princeton University. GLDASv2 is only produced through 2010, so we will only compare the earlier two years with the newer product. For both versions of GLDAS, the only LSM option is Noah, version 2.7, for GLDASv1 and Noah, version 3.3, for GLDASv2.

The Noah LSM is responsible for snowpack simulation in both versions of GLDAS and is available as an option in the North American Land Data Assimilation System (NLDAS). Multiple studies have considered the ability of Noah to estimate snow conditions (Pan et al. 2003; Sheffield et al. 2003). Nearly all studies show a tendency for Noah—whether in NLDAS, GLDAS, or as an offline LSM—to underestimate SWE (note that this is not the case for the most recent version of Noah, described later). Livneh et al. (2010) detail a negative SWE bias in Noah across the western United States, particularly in mountainous regions when compared to the Snowpack Telemetry (SNOTEL) network. Livneh et al. (2010) discuss techniques to decrease the SWE bias, including improvements to how Noah calculates albedo and allowing for refreeze within the snowpack. Other studies have identified similar biases in Noah snow simulations in a range of mountain environments (Barlage et al. 2010; Ek et al. 2003; Jin and Miller 2011; Sultana et al. 2014).

3) MERRA

The Modern-Era Retrospective Analysis for Research and Applications (MERRA) is an assimilation-based reanalysis product that incorporates NASA's

Earth Observing System satellite observations into a climate model framework (Rienecker et al. 2011). The data are available from the GES DISC (http://disc.sci.gsfc.nasa.gov/daac-bin/DataHoldings.pl) and are produced on a ½° × ⅔° grid (~55 × ~75 km), globally. Though evaluation of modeled grid cells against point measurements is inherently problematic because of issues of scale, MERRA snow depth estimates have been compared to in situ observations from the World Meteorological Organization (Reichle et al. 2011), with a correlation of 0.56 and a bias of −1.0 cm.

4) ERA-INTERIM

The European Centre for Medium-Range Weather Forecasts (ECMWF) interim reanalysis (ERA-Interim) is a global product at 0.75° resolution (~80 km; Dee et al. 2011) and is available for download (http://apps.ecmwf.int/datasets/data/interim-full-daily/). We use daily SWE estimates; note that the variable labeled "snow depth" in the ERA dataset is actually SWE, with units of meters of water equivalent (H. Garcon, ECMWF research team, 2015, personal communication). ERA-Interim has been shown to underpredict snowfall (Dutra et al. 2011) and predict melt too early in forested regions (Dutra et al. 2010). Kapnick and Delworth (2013) compiled a list of known biases in ERA-Interim snow estimates, including a negative SWE bias in coastal regions and missing snow in some midlatitude locations.

5) NLDAS

The NLDAS (Mitchell et al. 2004; Xia et al. 2012a,b) is a model reanalysis data product that is available from the GES DISC. We use the hourly data from the offline, uncoupled NLDAS phase 2 (NLDAS-2) runs, which are produced at 0.125°, or roughly ~14 km resolution. Forcing data for NLDAS come from the North American Regional Reanalysis (NARR; Mesinger et al. 2006), with the exception of the precipitation forcing, which is from the gauge network of the CPC and includes an orographic adjustment from the Parameter-Elevation Regressions on Independent Slopes Model (PRISM) climatology (Daly et al. 1994). NLDAS is run with three different LSMs: Mosaic (Koster and Suarez 1994, 1996); Noah, version 2.8 (Ek et al. 2003; Livneh et al. 2010; Wei et al. 2013); and VIC, version 4.0.3 (Liang et al. 1994; Wood et al. 1997; Sheffield et al. 2003). Here we compare results from NLDAS using each LSM, which we designate as NLDASvM (for NLDAS with Mosaic), NLDASvN (for NLDAS with Noah), and NLDASvV (for NLDAS with VIC). Additional information on the Noah and VIC LSMs can be found in Chen et al. (2014).

The NLDAS phase 1 had a negative bias in precipitation, which impacted estimation of both snow extent (Sheffield et al. 2003) and SWE (Pan et al. 2003). NLDAS-2 (Xia et al. 2012a,b) has updated forcing data, including the precipitation, and includes improved parameterizations in Noah for cold season processes (Livneh et al. 2010). Despite improvements, several of the LSMs within NLDAS still struggle to simulate reasonable streamflow cycles over snowy areas, and the lowest intermodel correlations occur over mountainous regions (Xia et al. 2012a,b).

6) CMC

The Canadian Meteorological Centre (CMC) produces daily snow depth estimates across the Northern Hemisphere at 24-km resolution (Brasnett 1999). Though snow depth values are available daily through assimilation of model results and in situ snow depth observations, SWE is only produced monthly, using monthly average snow depths with snow density estimates based on snow course measurements and snow classes from Sturm et al. (1995). The data are available from the NSIDC (Brown and Brasnett 2010) to compare to other products. Brown et al. (2003) show that, compared to snow course data, the CMC model tends to melt snow too quickly in the spring and leave too little snow cover in the high northern latitudes during the summer.

7) NARR

The NARR is an assimilation-based dataset that is available over North America, up to a latitude of ~85°N (Mesinger et al. 2006). Produced by the National Centers for Environmental Prediction, NARR estimates are available every 3 h at a resolution of 32 km and with 29 pressure levels. NARR data are available for download from the Research Data Archive from the National Center for Atmospheric Research (http://rda.ucar.edu/). Salzmann and Mearns (2012) evaluate NARR against SNOTEL observations across the upper Colorado River basin. NARR reaches peak SWE too early, up to 3 months prior to the SNOTEL SWE peak, and does not demonstrate a clear annual cycle of SWE, but rather accumulates and melts snow multiple times throughout the season. Salzmann and Mearns (2012) suggest that NARR was designed to estimate snow cover, not SWE, possibly explaining the poor correlation between NARR and SNOTEL SWE (R^2 = 0.16). Here we not only compare NARR to the other data products, but we also use NARR as forcing data for WRF.

8) SNODAS

SNODAS (Carroll et al. 2001; National Operational Hydrologic Remote Sensing Center 2004), developed by the National Weather Service, provides daily estimates of SWE over the continental United States at a resolution of

1 km. As an assimilation-based dataset, SNODAS updates model predictions with satellite observations of snow cover fraction, gamma radiation airborne measurements, radar precipitation observations, and in situ measurements. The in situ measurements, such as snow pillows and snow courses, are used in the assimilation algorithm where applicable, causing SNODAS to perfectly match the in situ observations in some cases. As an operational data product, no documentation describing the details of the methodology is available, though several studies have evaluated the product against limited field observations and models. Clow et al. (2012) compare SNODAS SWE estimates to both ground-based field surveys and stream gauges in the Colorado Rockies. Though SNODAS performed well in forested areas and was capable of explaining 77% of the variance in SWE, the product did not fare as well in alpine areas and only explained 30% of the variance. Hedrick et al. (2015) found similar biases for SNODAS in alpine regions when they compared SNODAS snow depth estimates to lidar measurements over the Cold Land Processes Field Experiment sites in Colorado, with a root-mean-square difference of 13 cm for snow depth over 12 study areas. Hedrick et al. (2015) note that SNODAS underpredicts snow depth in regions with deep snowpack and dense forests, both of which are common characteristics of mountain environments.

9) SWE reanalysis

The SNSR provides daily estimates of SWE at a spatial resolution of 90 m. The reanalysis uses a data assimilation framework to constrain and update model-based SWE estimates using Landsat fractional snow-covered area images. Model inputs include meteorological forcing from the NLDAS-2 dataset (described above); the SNSR explicitly treats the uncertainty in the forcing dataset and model parameterizations, producing an optimal SWE estimate constrained by the Landsat imagery. Note that SNSR is computed independently from in situ SWE measurements and is only compared against them for validation purposes. The method models the effect of forests on snow accumulation and ablation, although validation is only possible against the snow pillows and snow courses observations that are made in unforested areas. At the watershed scale, the reanalysis accuracy shows a weak, statistically insignificant dependence on forest cover fraction, suggesting that forest cover does not greatly impact the reanalysis algorithm. The SNSR product was verified against over 9000 station years of snow pillow and course data over the period 1985–2015; bias was less than 3 cm, root-mean-square error was less than 13 cm, and R was greater than 0.95 (Margulis et al. 2016).

4. Methods

a. WRF Model simulations

We ran WRF, version 3.6 (Skamarock et al. 2008), with the Noah LSM with multiparameterization (Noah-MP; Niu et al. 2011); the Noah-MP snow model improvements over the Noah snow model are described below. All simulations are run with three one-way nested domains at increasingly fine resolution: 27, 9, and 3 km. The outermost domain receives forcing data from NARR. Prior work suggests that a resolution of ~3 km is necessary to capture orographic processes to first order (Pavelsky et al. 2011; Wrzesien et al. 2015). However, we will consider how the SWE simulations differ among the three WRF resolutions. The 27-, 9-, and 3-km domains are described as WRF27km, WRF9km, and WRF3km, respectively.

We select the following physics options when running WRF: the Thompson et al. (2004) cloud microphysics scheme, the Rapid Radiative Transfer Model longwave scheme (Mlawer et al. 1997), the Dudhia shortwave scheme (Dudhia 1989), the Yonsei University planetary boundary layer scheme (Hong et al. 2006), and the modified Kain–Fritsch convective parameterization for the two outer domains (Kain 2004; Kain and Fritsch 1990, 1993). All options are consistent with previous studies on the Sierra Nevada (Pavelsky et al. 2011, 2012; Wrzesien et al. 2015).

Here we use all default options for Noah-MP, including turning off dynamic vegetation, using the Canadian Land Surface Scheme (CLASS; Verseghy 1991) to calculate snow albedo, and partitioning rain and snow using the Jordan (1991) algorithm. The CLASS algorithm calculates snow surface albedo through a combination of fresh snow albedo and snow age. The Jordan (1991) partitioning scheme uses a function based on air temperature, with a large decrease in the percent of frozen precipitation between 1° and 2°C. This is in line with Lundquist et al. (2008), who use a threshold of 1.5°C to partition between rain and snow in the Sierra Nevada. Perhaps the most important improvement from Noah to Noah-MP is that Noah-MP has a multilayer snowpack. Models with multiple snow layers allow for more accurate snow surface temperature simulation, which allows for more accurate outgoing longwave simulation (Etchevers et al. 2004).

There are numerous studies using WRF to estimate mountain snow (e.g., Leung and Qian 2003; Caldwell et al. 2009; Keighton et al. 2009; Ikeda et al. 2010; Rasmussen et al. 2011; Maussion et al. 2011). Pavelsky

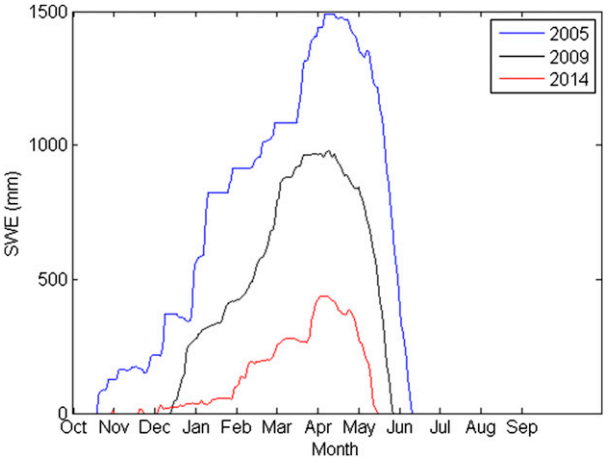

FIG. 2. Accumulation over the water year for GOL station, a snow pillow at Gold Lake, a location in the Feather River basin in the northern Sierra Nevada. Daily SWE is shown for water years 2005 (blue), 2009 (black), and 2014 (red).

et al. (2011) evaluate the abilities of WRF, run with the older Noah LSM, to simulate snow dynamics over the central Sierra Nevada. Comparing to both snow and meteorological observations, they find that the WRF run at 3 km simulates snow melt 22–25 days too early and that simulated temperatures tend to be too cold, with an overall mean bias of −2.6°C. Pavelsky et al. (2011) also show that WRF with Noah is capable of reproducing precipitation timing, but the total precipitation is biased high by nearly 12%, though only 10 sites are compared. Correlation between modeled temperatures at 3-km WRF grid cells and measured temperatures at 31 meteorological stations is 0.88. To address the early melt bias, Wrzesien et al. (2015) ran WRF with the improved Noah-MP LSM for the same time and domain. With the newer LSM, the melt bias is reduced to 2 days and at the mountain range scale, WRF is capable of identifying the presence/absence of snow when compared to a satellite-derived snow product. Additionally, Wrzesien et al. (2015) show that WRF with Noah-MP has a peak SWE bias of 8.37 cm compared to snow pillow measurements. Other studies (Niu et al. 2011; Cai et al. 2014) have also shown improvements in snow modeling and terrestrial water storage estimates in Noah-MP, as compared to Noah.

b. *Interpolation*

To produce an interpolation based on in situ observations, we regress SWE from snow courses against latitude, longitude, elevation, slope, aspect, average winter temperature, and total winter precipitation (Carroll and Cressie 1997; Fassnacht et al. 2003). Temperature and precipitation are from PRISM (http://www.prism.oregonstate.edu), while elevation data and their derivatives are from the U.S. Geological Survey's global 30 arc s elevation dataset (GTOPO30; https://lta.cr.usgs.gov/GTOPO30). The interpolation was performed at 4-km resolution, matching the PRISM resolution. Following Howat and Tulaczyk (2005), we krige the residuals over the entire domain and add the interpolated residuals to the trend surface to produce a final SWE interpolation over the Sierra Nevada. To prevent snow cover from unrealistically extending too far downslope, we mask out areas below 1500 m elevation, the approximate average snow line in the Sierra Nevada (Shamir and Georgakakos 2006; Lundquist et al. 2008).

5. Experiment design

We compare the global/CONUS+ and WRF range-wide SWE against reference SWE datasets. These include the SNSR (which is independent from, but validated against, snow pillows and snow courses), the interpolation (based on snow courses), and SNODAS (which assimilates snow pillows). These three datasets represent completely different approaches, in terms of their methodology, ranging from operational (SNODAS) to the relatively simple interpolation to the relatively complex SNSR. We consider an average of the reference datasets and evaluate the consistency between the three products.

We consider three water years—2005, 2009, and 2014—to represent high, average, and low snow accumulation, respectively [readers should consider Margulis et al. (2016) for a 31-yr record of Sierra Nevada SWE to understand how the selected years relate to each other and to other years in the record]. Figure 2 shows SWE accumulation at a representative station, the Gold Lake snow pillow (elevation of 2057 m), for these three years (Kapnick and Hall 2010). Though we do not consider individual storm tracks for each year, future work should analyze storm tracks and their effects on SWE accumulation, which could reveal biases in the gridded SWE estimates (Lundquist et al. 2015). We consider SWE time series from each data product, along with 1 April SWE, peak SWE, and peak SWE timing. The date 1 April is analyzed because it is a common metric in the literature and close to snow course measurement dates. For pentad (AMSR-E) or monthly (CMC) datasets, we select the date range that includes 1 April. Peak SWE provides the total snow storage for each dataset, while peak SWE timing shows how accumulation over the winter differs between the data products.

6. Research questions and hypotheses

Our overarching research question is, can existing datasets available to the community or WRF simulations

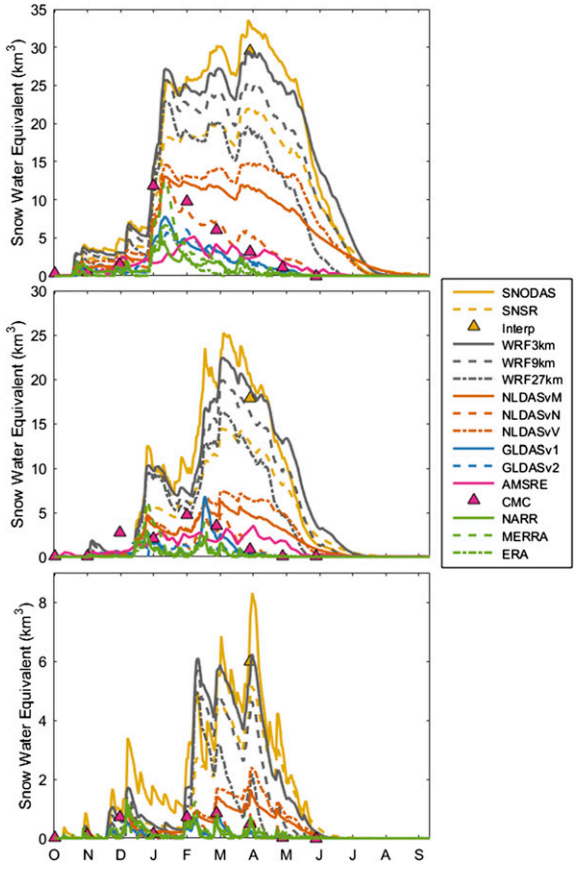

FIG. 3. Time series of SWE for each dataset for water year (top) 2005, (middle) 2009, and (bottom) 2014.

produce estimates of total mountain range SWE within an uncertainty of ±50%, relative to the reference SWE datasets? We choose ±50% as representative of the precision required to quantify SWE to the first significant figure in the construction of continental and global water and energy budgets. More specifically, our study is motivated by three questions: Are the reference SWE datasets consistent with each other? If so, are the global or CONUS+ estimates consistent with the reference? Finally, is WRF, a high-resolution RCM, consistent with the reference?

Based on their past performance, we expect global datasets to have an overall lower amount of SWE as compared to the reference datasets. We expect both versions of GLDAS to underestimate SWE because of the biases in the Noah LSM described above. We also expect ERA-Interim and MERRA to underestimate SWE because of poor resolution of topography. We hypothesize that AMSR-E cannot estimate SWE within ±50%, consistent with the numerous studies that discuss the deficiencies of its algorithm in mountain environments.

We similarly expect these models and observations to underestimate SWE for the CONUS+ products. Despite the improvements from NLDAS-1 to NLDAS-2, prior work suggests that the LSMs in NLDAS-2 still struggle in complex environments, so we believe that the NLDAS-2 estimates presented here will underestimate SWE, and we do not necessarily expect a consensus between the three LSMs. Since NARR is not optimized for SWE, we expect it to behave as one of the poorer datasets. Finally, CMC is likely the most reasonable where the in situ network is densest; with observations in mountainous regions being comparatively sparse, we hypothesize that the CMC estimate will be too low.

Based on previous studies with WRF (Pavelsky et al. 2011; Wrzesien et al. 2015; Leung and Qian 2003; Ikeda et al. 2010; Rasmussen et al. 2011), we hypothesize that high-resolution WRF simulations will produce reasonable peak SWE, 1 April SWE, and peak SWE timing, when compared to the reference datasets.

7. Results

a. Temporal analysis

Figure 3 shows SWE time series throughout each water year for all datasets. Range-wide, distinct accumulation and ablation seasons are less evident than they are for the single-station, high-elevation SWE time series (e.g., that shown in Fig. 2, with an elevation of 2057 m). Instead, ablation occurs intermittently throughout the winter, following each accumulation event; this is especially evident for 2009 and 2014. While the timing of major accumulation and ablation events is similar across all datasets, there are dramatic differences in the magnitude of accumulation and melt events. For example, in 2005, most datasets have a large accumulation event in January; however, the reference datasets and the WRF estimates show ~25–30 km^3 of new accumulated SWE, while all other datasets have only ~5–15 km^3. After the January 2005 accumulation event, melt occurs as demonstrated in nearly all datasets (except AMSR-E). SWE in the reference datasets decreases by 15%–20% with similar values for the WRF estimates. MERRA, on the other hand, simulates a large melt event, with SWE decreasing by >40% in less than a month. Alternatively, NLDAS products show SWE persisting too late in the year, with slow ablation rates compared to the reference datasets. For all three years, WRF SWE time series are similar to the reference estimates, while the global/CONUS+ datasets greatly underestimate SWE.

While 1 April is often used as a peak SWE proxy, that date is not always indicative of peak accumulation, as

TABLE 1. Date on which each dataset reaches peak SWE for each water year.

Data product	2005	2009	2014
SNSR	30 Mar	6 Mar	2 Apr
SNODAS	30 Mar	7 Mar	3 Apr
WRF3km	30 Mar	6 Mar	3 Apr
WRF9km	12 Jan	6 Mar	11 Feb
WRF27km	12 Jan	6 Mar	10 Feb
NLDASvM	12 Jan	5 Mar	1 Apr
NLDASvN	12 Jan	5 Mar	1 Mar
NLDASvV	30 Mar	5 Mar	2 Apr
NARR	8 Jan	26 Dec	7 Dec
AMSR-E	5 Feb	1 Apr	—
GLDASv1	11 Jan	18 Feb	1 Mar
GLDASv2	31 Jan	31 Dec	—
MERRA	11 Jan	26 Dec	7 Dec
ERA-Interim	12 Jan	26 Dec	10 Dec

seen here for 2009. The dates of peak SWE for each year and each dataset are shown in Table 1, with 2014 dates ranging from as early as 7 December for NARR and MERRA to as late as 3 April for SNODAS and WRF3km. The two reference datasets with daily data (SNSR and SNODAS) are in near-perfect agreement for the date of peak SWE across all three years. For two of the three years (2005 and 2014), 1 April is an approximate estimate of the actual date of peak SWE. Related to the goals of this study of evaluating global/CONUS+ data products and WRF simulations against reference datasets, the SWE time series indicate that the relative difference between datasets for range-wide SWE is similar for 1 April and for peak SWE. In the rest of the analysis, we focus on 1 April SWE, particularly since peak SWE is not available for all datasets (i.e., CMC and the interpolation).

b. 1 April spatial analysis

Figures 4–6 show the spatial distribution and extent of the 1 April SWE for each dataset for water years 2005, 2009, and 2014, respectively. The reference datasets show similar spatial distributions of SWE. Visually, the SNSR, with gridcell resolution over an order of magnitude finer than the next closest product, demonstrates features not shown by other datasets. For example, there is a slight maximum in SWE in all three years on the northeastern shore of Lake Tahoe. When comparing Figs. 4–6 (bottom), SNSR has fewer large areas with high SWE values. The interpolation, in contrast, shows large areas with >1000 mm of SWE. The snow extent of the interpolation is larger than either the SNSR or SNODAS for all three years. Nonetheless, these three products show similar spatial patterns of SWE each year.

The global products (Figs. 4–6, top) show lower SWE values and decreased snow extent than the reference datasets on 1 April for all years. AMSR-E underestimates snow extent over the entire domain, but particularly in the northern portion of the domain, perhaps due to more expansive forest cover. Both versions of GLDAS fail to estimate any snow in the northern Sierra Nevada for all three years, as is particularly evident in the high snow year of 2005 (Fig. 4). Finally, the two coarsest global products, MERRA and ERA-Interim, show little to no snow in the Sierra Nevada on 1 April. Similarly, all CONUS+ datasets (Figs. 4–6, middle) estimate relatively little snow on 1 April, in comparison with the reference datasets. In particular, all three of the NLDAS products show little-to-no snow in the northern portion of the mountain range. Both CMC and NARR suggest very little snow throughout the Sierra Nevada on 1 April.

When only considering 1 April SWE distribution, the WRF3km and WRF9km are the most similar to the reference among all of the datasets, though differences do exist. There are more high snow regions (SWE > 1000 mm) in WRF3km than in the SNSR, and WRF9km predicts too much snow cover in the far northern part of the domain.

c. 1 April range-wide SWE

SWE volume in the Sierra Nevada across all years and datasets is shown in Fig. 7. In all three study years, the 1 April SWE estimates from the reference datasets are consistent and within ±50% of the reference mean. In fact, no single-year estimate for any of the datasets differs from the mean by more than 21%. Similarly, for the peak SWE estimate, where only the SNSR and SNODAS are available, reference dataset SWE values are within ±50% of the reference mean. For each year, the SNSR has the smallest SWE estimate of the reference datasets, SNODAS produces the largest estimate, and the interpolation falls between the other two reference datasets.

With the exception of AMSR-E, all global products produce 1 April SWE estimates $<1\,km^3$. Surprisingly, AMSR-E has the largest SWE estimate of all the global products, despite the disadvantages of passive microwave in mountainous regions. However, the AMSR-E SWE estimates—and the rest of the global datasets—are far lower than the reference dataset estimates. For example, the 2005 SWE from AMSR-E is only 9% the reference mean. The CONUS+ estimates, despite resolutions finer than the global products, still produce much less SWE than the reference estimates. NLDASvV, for example, is the closest of the CONUS+ products to the reference datasets (e.g., NLDASvV for 2005 is 54% of the reference mean), but all three versions of NLDAS produce substantially less SWE than

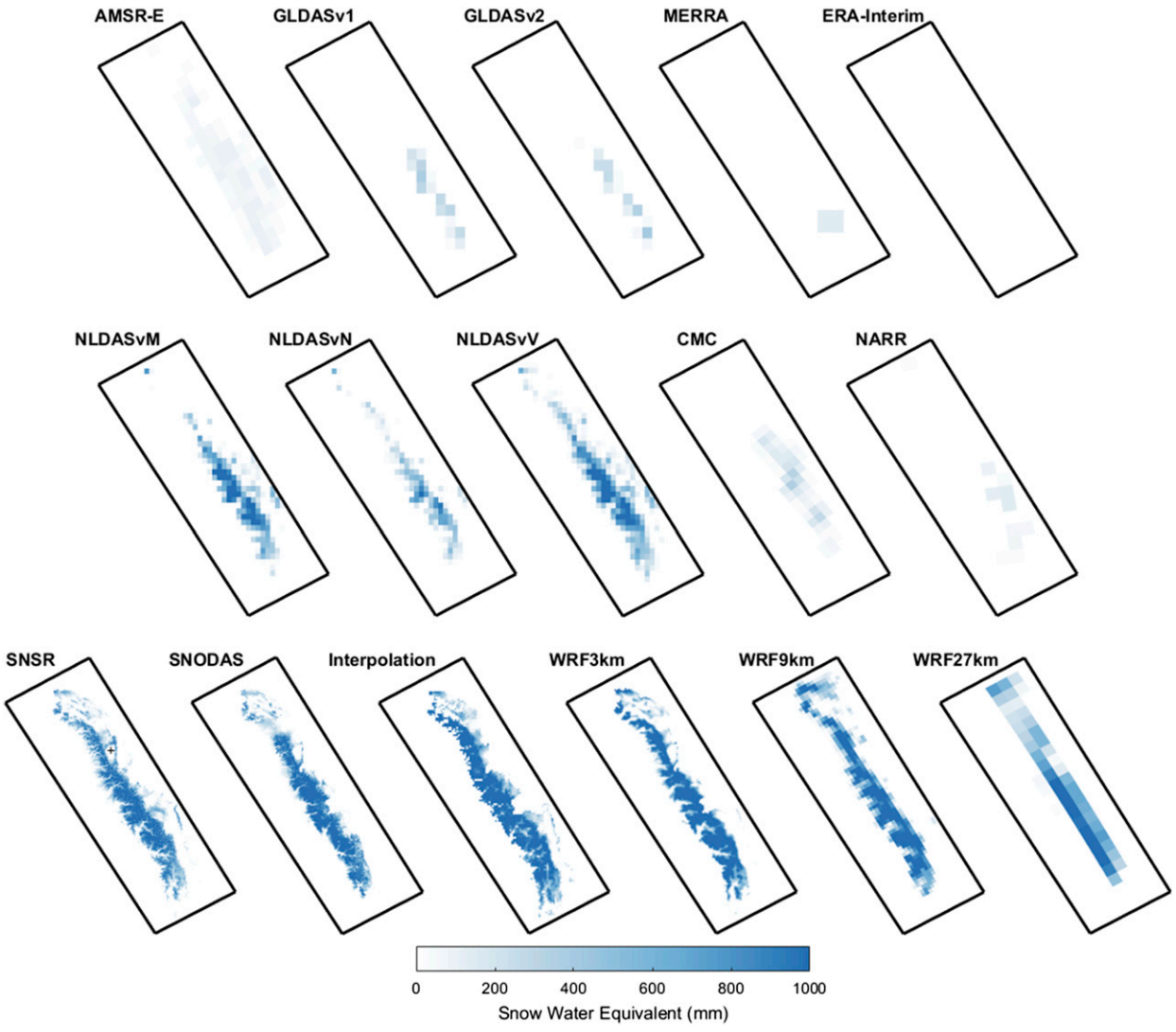

FIG. 4. Simulated SWE for (top) global products (AMSR-E, GLDASv1, GLDASv2, MERRA, and ERA-Interim), (middle) CONUS+ products (NLDASvM, NLDASvN, NLDASvV, CMC, and NARR), and (bottom) reference datasets and WRF (SNSR, SNODAS, Interpolation, WRF3km, WRF9km, and WRF27km) for 1 Apr 2005. SWE values sometimes exceed the color map max of 1000 mm. The plus sign on the SNSR plot indicates Lake Tahoe.

the reference datasets. CMC and NARR 1 April SWE estimates are even lower than the NLDAS estimates.

Finally, we compare the WRF SWE estimates to the references. WRF3km is the most similar in total overall SWE with the reference datasets, with values that are 97%, 104%, and 84% of the reference mean for 2005, 2009, and 2014, respectively. Similarly, the WRF9km estimate is 91%, 100%, and 72% of the reference mean for 2005, 2009, and 2014, respectively. For 2005, 2009, and 2014, the WRF27km 1 April SWE estimate is 70%, 74%, and 30% of the reference mean, respectively.

Overall, the global/CONUS+ products tend to show very little SWE, with values approximately an order of magnitude smaller than the reference products. Of the products with resolution of >20 km (CMC, AMSR-E, WRF27km, GLDASv1, GLDASv2, NARR, MERRA, and ERA-Interim), only WRF27km is somewhat comparable to the reference estimates.

8. Discussion

a. Evaluating the research questions

We first explore the consistency of the three reference datasets (SNODAS, the snow course interpolation, and the SNSR). All three are relatively consistent with each other, producing an "average" year 1 April SWE for 2009 ranging from 12.8 to 17.9 km^3, with the SNODAS and interpolation estimates being ~39% larger than the SNSR

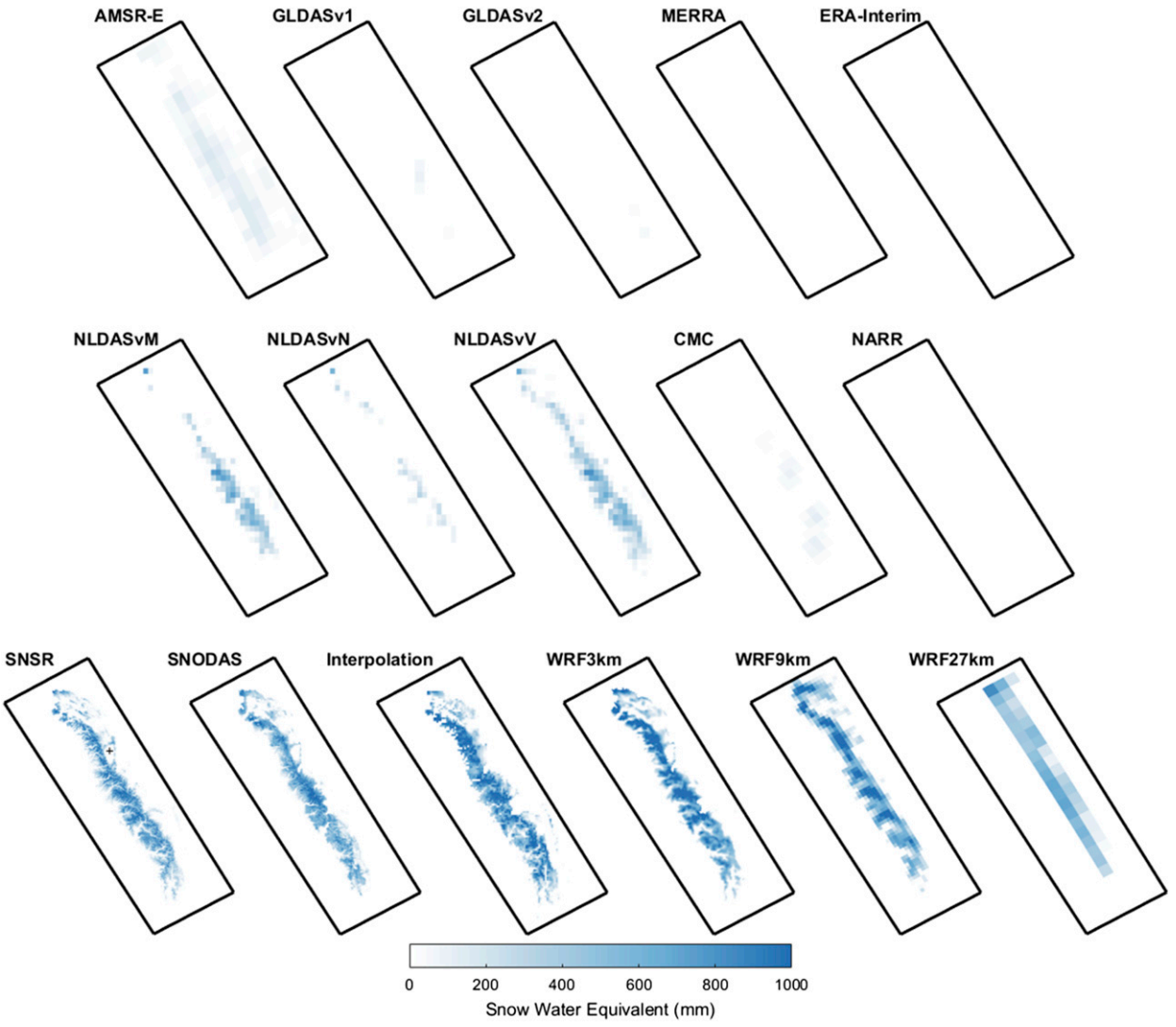

FIG. 5. As in Fig. 4, but for 2009.

estimate of 12.8 km^3. Fractional differences among the three reference datasets are similar for each water year. We see little evidence of SWE underestimation in SNODAS estimates, unlike previous studies (Hedrick et al. 2015). Despite differences in each reference dataset, all estimate SWE to within ±21% of the reference mean, well below the ±50% "reasonable" threshold we suggest here. Therefore, we suggest that our three reference datasets—SNSR, the interpolation, and SNODAS—are approximately consistent with one another. The reference estimates presented here are also in agreement with previously published SWE values (Table 2).

In contrast, we determine that the global/CONUS+ products are not in agreement with the reference products. Only one year of NLDASvV is within ±50% of the 1 April reference mean (at 54% for 2005); for 2009 and 2014, no global/CONUS+ dataset is within ±50%. The same results hold true for peak SWE, though here the reference average includes only the SNSR and SNODAS. From these results, it seems that coarser-resolution datasets are inadequate to characterize Sierra Nevada snow accumulation, perhaps since the Sierra Nevada is a narrow mountain range. Some of the products, such as GLDAS, MERRA, and ERA-Interim, are commonly used in larger-scale studies (e.g., Syed et al. 2008; Meng et al. 2012; Mankin et al. 2015), yet they considerably underpredict the amount of snow in the Sierra Nevada (Fig. 3). Additionally, as would be expected from past studies, the AMSR-E passive microwave product derived from spectral gradients does not perform well over the Sierra Nevada since complex topography, deep snowpack, and high forest fraction combine to produce poor microwave

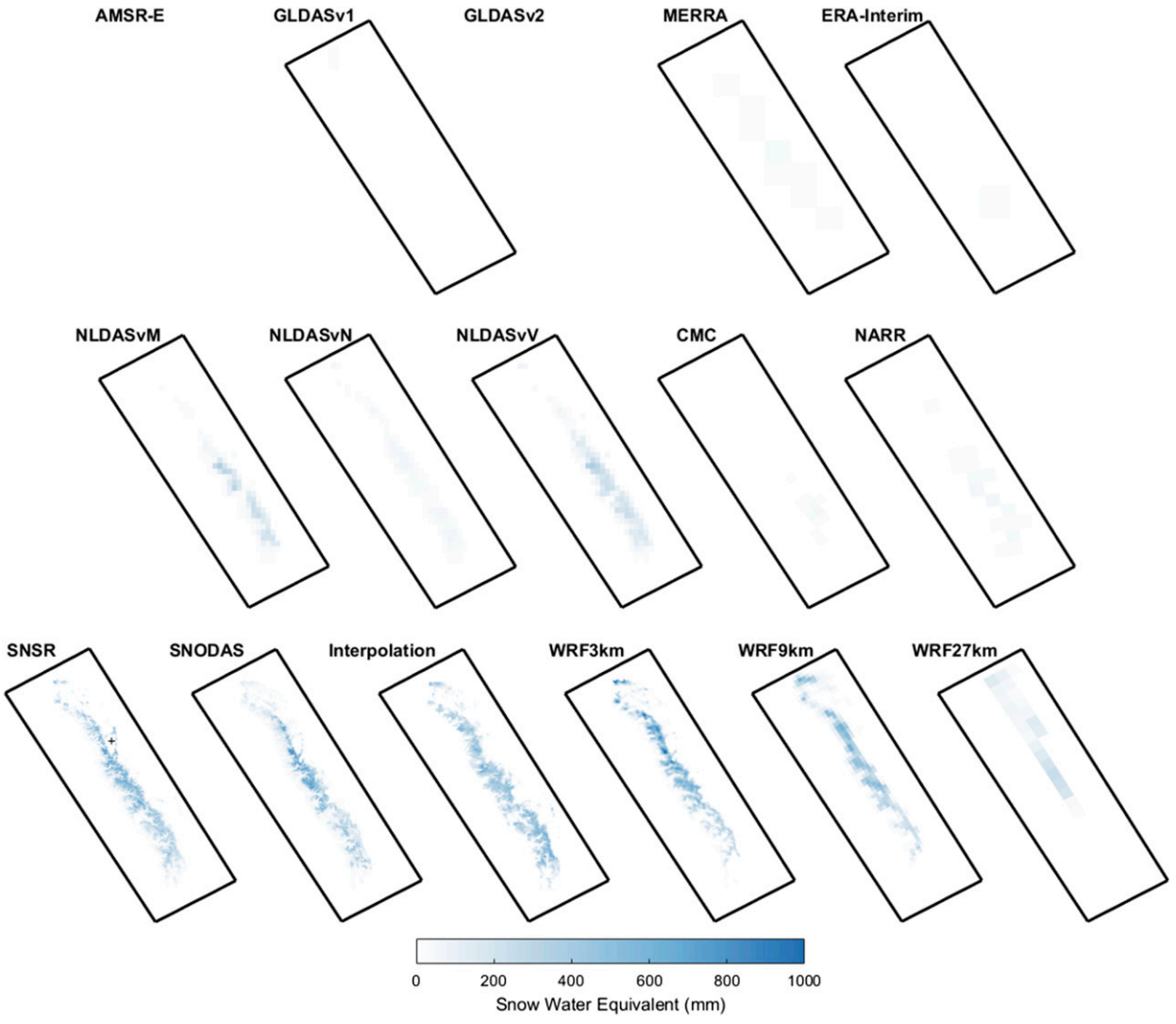

FIG. 6. As in Fig. 4, but for 2014. For 2014, data are unavailable for AMSR-E and GLDASv2.

retrievals (Vuyovich et al. 2014). Even when considering the potential biases of in situ observations, which could result in overprediction of range-scale SWE, it is highly unlikely that any of the global/CONUS+ datasets produce realistic amounts of snow in the Sierra Nevada.

Finally, we compare WRF to the reference datasets. For all three years, both WRF3km and WRF9km estimates for 1 April SWE are within ±50% of the estimates from the reference datasets. WRF27km is also within ±50% for 2005 and 2009. The same is true for peak SWE. In fact, WRF27km is the dataset that is the closest to the SNSR 1 April estimate for both 2005 and 2009 (WRF3km is closest in 2014).

b. *Roles of mass and energy balance*

Visualizing how SWE evolves throughout the year (Fig. 3) demonstrates the differences among the datasets. When only considering the three WRF estimates (gray lines), the effect of resolution is apparent. Other than parameterizations for convection (which the 3-km domain explicitly resolves), the only difference between the three WRF estimates is gridcell size. As grid size increases from 3 to 9 to 27 km, the amount of SWE decreases. The three datasets are most similar during the early part of the accumulation season, but once melt begins, even in midwinter, the estimates diverge. While WRF3km does estimate more total accumulation than WRF27km (<20% more in 2005 and 2009, 40% for 2014), the differences in accumulation cannot fully explain the overall SWE differences between the three model resolutions. Variation between high- and low-resolution WRF estimates are at least as much driven by ablation processes as they are by accumulation. For example, in 2005, WRF3km and WRF9km have

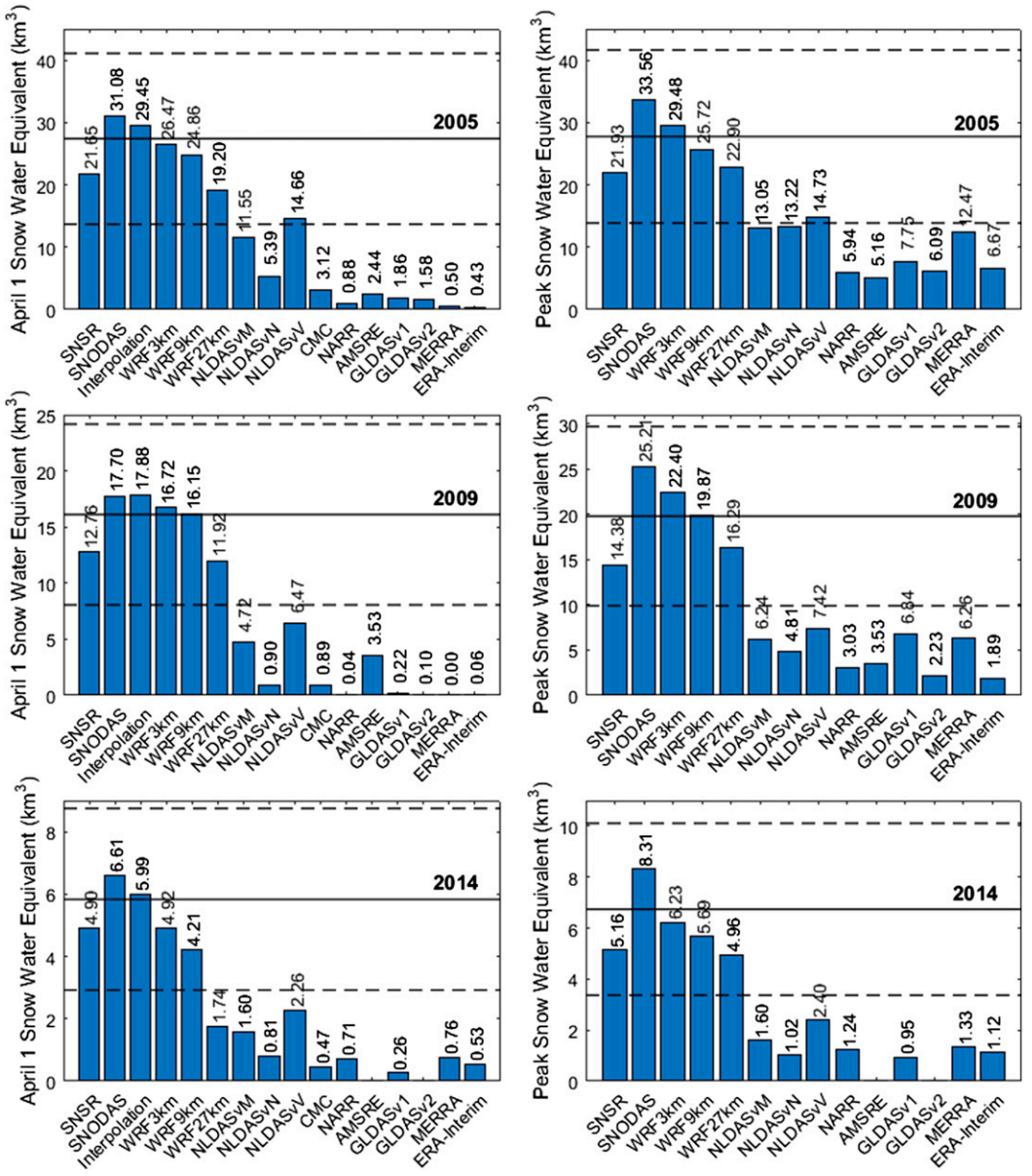

FIG. 7. SWE volume (km^3) for each gridded dataset for (left) 1 Apr SWE and (right) peak SWE for (top) 2005, (middle) 2009, and (bottom) 2014. Solid black line indicates the reference dataset average and the dashed lines show ±50% of the reference mean.

relatively constant SWE, despite minor accumulation and ablation events, yet WRF27km has a general decline beginning in January (Fig. 3). Similarly, in 2014, WRF3km fluctuates around 5 km^3 between February and April, WRF9km has a slow decline, and WRF27km has a rapid decline. This perhaps indicates not only a bias in precipitation at the coarser resolution but also in the energy balance, possibly due to radiation differences associated with smoothed elevation in the larger grid cells.

In some of the other products, a bias in the energy balance is more evident. For example, for water year 2005 (Fig. 3, top), MERRA (dashed light green line) accumulates snow up until 11 January and then experiences a large melt event that far surpasses the melt in any other product. Rain–snow partitioning could also be a problem in some of the datasets. For example, for 2009, in WRF, 44% of the precipitation falls as snow, but in MERRA, only 32% is snowfall. Regardless of whether MERRA produces enough

TABLE 2. Estimates of Sierra Nevada SWE (km^3) from the literature.

Reference	Study period	SWE (km^3)
Howat and Tulaczyk (2005)	1 Apr for 1950 to 2002	25 (estimated from their Fig. 5)
Hayhoe et al. (2004)	Avg 1 Apr SWE from 1961 to 1990	12.4
Margulis et al. (2016)	Avg 1 Apr SWE from 1985 to 2015	14.2

precipitation, uncertainties in the energy balance calculation result in snow melting out too quickly and too early. Alternatively, the NLDAS products, particularly NLDASvM and NLDASvV, delay snowmelt for too long compared to the rest of the estimates. This, again, is likely due to biases in the energy balance. Table 1 shows the date of peak SWE for each dataset in all three water years. WRF3km agrees with the reference in all three years. Surprisingly, NLDASvV matches the peak SWE timing, but it does not accumulate enough snow. All other datasets differ substantially, at least for one year, including both WRF9k and WRF27km. Only WRF3km is similar to the reference datasets in both SWE magnitude and peak SWE timing (Figs. 3, 7).

An interesting finding is that the WRF27km SWE estimate compares relatively well to the finer-spatial-resolution SWE estimates, particularly the SNSR for 2005 and 2009. Though spatial resolution is important for realistic simulation of temperature lapse rates and orographic precipitation, it is clearly not the only important factor in obtaining realistic SWE estimates. Indeed, WRF27km produces more reasonable estimates than the finer-resolution NLDAS estimates. Other factors may include differences in rain–snow partitioning or the fact that WRF is a coupled atmosphere–land model and is thus able to account for feedbacks from the land surface to the atmosphere through the LSM, Noah-MP (Niu et al. 2011). Additionally, Noah-MP is an improvement over the Noah LSM (used in both versions of GLDAS and in NLDASvN) since Noah-MP simulates the snowpack using up to three layers (as opposed to one layer in Noah) and has separate energy fluxes for vegetated and nonvegetated surfaces. Recent analysis suggests that Noah-MP simulates snowmelt processes more realistically than does Noah (Niu et al. 2011; Wrzesien et al. 2015; Pavelsky et al. 2011). We hypothesize that better simulations of the mass and energy balances through these factors lead to more realistic WRF27km SWE estimates than would be expected from its spatial resolution alone.

9. Conclusions

Using the California Sierra Nevada, we show that three reference datasets—the SNSR, SNODAS, and a snow course interpolation—produce consistent estimates of total range-wide SWE (within ±21% of their mean), and that currently available global/CONUS+ products inadequately estimate mountain range SWE. Global products such as GLDAS, MERRA, and ERA-Interim produce unreasonable estimates that are up to an order of magnitude less than some of the more reasonable data products, such as the SNSR and SNODAS. We further show that the WRF RCM produces estimates of mountain peak SWE and timing for the Sierra Nevada that are within ±27% of the reference datasets, well within the ±50% threshold.

The ability of the WRF RCM to approximate montane SWE is encouraging. The perhaps surprising adequacy of WRF at both 3- and 9-km resolutions in simulating pan–Sierra Nevada SWE accumulation opens new possibilities for estimating mountain snowpack outside of well-monitored areas. SNODAS is available only for the continental United States. While the Sierra Nevada has a relatively dense in situ gauge network, spanning many of the major climatic and physiographic gradients in the mountain range, the majority of global complex topography does not. Simply put, interpolations are not possible in most mountain ranges. Compared to ultrafine-resolution SWE estimates, such as the SNSR, WRF estimates can be processed over areas with few observational datasets. At fine resolution (<9 km), orographic processes are captured and SWE estimates compare favorably to reference datasets, which are based on/validated against in situ observations. Therefore, we recommend large-scale future studies focused on mountain hydrology should use RCMs as opposed to currently available datasets, such as ERA-Interim, GLDAS, or even NLDAS.

Acknowledgments. M. L. Wrzesien is funded by NASA Earth and Space Science Fellowship NNX14AT34H. M. T. Durand is funded in part by NASA New Investigator Grant NNX13AB63G. We would like to acknowledge high-performance computing support from Yellowstone (ark:/85065/d7wd3xhc) provided by NCAR's Computational and Information Systems Laboratory, sponsored by the National Science Foundation. The authors would also like to thank Anne Nolin and an anonymous reviewer for helpful comments which greatly added to the manuscript.

REFERENCES

Barlage, M., and Coauthors, 2010: Noah land surface model modifications to improve snowpack prediction in the Colorado Rocky Mountains. *J. Geophys. Res.*, **115**, D22101, doi:10.1029/2009JD013470.

Barnett, T. P., J. C. Adam, and D. P. Lettenmaier, 2005: Potential impacts of a warming climate on water availability in snow-dominated regions. *Nature*, **438**, 303–309, doi:10.1038/nature04141.

Blöschl, G., 1999: Scaling issues in snow hydrology. *Hydrol. Processes*, **13**, 2149–2175, doi:10.1002/(SICI)1099-1085(199910)13:14/15<2149::AID-HYP847>3.0.CO;2-8.

Brasnett, B., 1999: A global analysis for snow depth for numerical weather prediction. *J. Appl. Meteor.*, **38**, 726–740, doi:10.1175/1520-0450(1999)038<0726:AGAOSD>2.0.CO;2.

Brown, R. D., and B. Brasnett, 2010: Canadian Meteorological Centre (CMC) daily snow depth analysis data, version 1. Updated daily, NASA National Snow and Ice Data Center Distributed Active Archive Center, accessed 6 January 2017, doi:10.5067/W9FOYWH0EQZ3.

——, ——, and D. Robinson, 2003: Gridded North American monthly snow depth and snow water equivalent for GCM evaluation. *Atmos.–Ocean*, **41**, 1–14, doi:10.3137/ao.410101.

Cai, X., Z.-L. Yang, Y. Xia, M. Huang, H. Wei, L. R. Leung, and M. B. Ek, 2014: Assessment of simulated water balance from Noah, Noah-MP, CLM, and VIC over CONUS using the NLDAS test bed. *J. Geophys. Res. Atmos.*, **119**, 13 751–13 770, doi:10.1002/2014JD022113.

Caldwell, P., H.-N. S. Chin, D. C. Bader, and G. Bala, 2009: Evaluation of a WRF dynamical downscaling simulation over California. *Climatic Change*, **95**, 499–521, doi:10.1007/s10584-009-9583-5.

Carroll, S. S., and N. Cressie, 1997: Spatial modeling of snow water equivalent using covariances estimated from spatial and geomorphic attributes. *J. Hydrol.*, **190**, 42–59, doi:10.1016/S0022-1694(96)03062-4.

Carroll, T., D. Cline, G. Fall, A. Nilsson, L. Li, and A. Rost, 2001: NOHRSC operations and the simulation of snow cover properties for the conterminous U.S. *Proc. 69th Annual Meeting of the Western Snow Conf.*, Sun Valley, ID, Western Snow Conference, 14 pp. [Available online at www.westernsnowconference.org/sites/westernsnowconference.org/PDFs/2001Carroll.pdf.]

Chen, F., and Coauthors, 2014: Modeling seasonal snowpack evolution in the complex terrain and forested Colorado Headwaters region: A model intercomparison study. *J. Geophys. Res. Atmos.*, **119**, 13 795–13 819, doi:10.1002/2014JD022167.

Clark, M. P., and Coauthors, 2011: Representing spatial variability of snow water equivalent in hydrologic and land-surface models: A review. *Water Resour. Res.*, **47**, W07539, doi:10.1029/2011WR010745.

Cline, D. W., R. C. Bales, and J. Dozier, 1998: Estimating the spatial distribution of snow in mountain basins using remote sensing and energy balance modeling. *Water Resour. Res.*, **34**, 1275–1285, doi:10.1029/97WR03755.

Clow, D. W., L. Nanus, K. L. Verdin, and J. Schmidt, 2012: Evaluation of SNODAS snow depth and snow water equivalent estimates for the Colorado Rocky Mountains, USA. *Hydrol. Processes*, **26**, 2583–2591, doi:10.1002/hyp.9385.

Daly, C., R. P. Neilson, and D. L. Phillips, 1994: A statistical–topographic model for mapping climatological precipitation over mountainous terrain. *J. Appl. Meteor.*, **33**, 140–158, doi:10.1175/1520-0450(1994)033<0140:ASTMFM>2.0.CO;2.

Dee, D. P., and Coauthors, 2011: The ERA-Interim reanalysis: Configuration and performance of the data assimilation system. *Quart. J. Roy. Meteor. Soc.*, **137**, 553–597, doi:10.1002/qj.828.

Done, J., C. A. Davis, and M. Weisman, 2004: The next generation of NWP: Explicit forecasts of convection using the weather research and forecasting (WRF) model. *Atmos. Sci. Lett.*, **5**, 110–117, doi:10.1002/asl.72.

Dozier, J., E. H. Bair, and R. E. Davis, 2016: Estimating the spatial distribution of snow water equivalent in the world's mountains. *Wiley Interdiscip. Rev.:Water*, **3**, 461–474, doi:10.1002/wat2.1140.

Dudhia, J., 1989: Numerical study of convection observed during the winter monsoon experiment using a mesoscale two-dimensional model. *J. Atmos. Sci.*, **46**, 3077–3107, doi:10.1175/1520-0469(1989)046<3077:NSOCOD>2.0.CO;2.

Durand, M., and S. A. Margulis, 2007: Correcting first-order errors in snow water equivalent estimates using a multifrequency, multiscale radiometric data assimilation scheme. *J. Geophys. Res.*, **112**, D13121, doi:10.1029/2006JD008067.

——, E. J. Kim, and S. A. Margulis, 2009: Radiance assimilation shows promise for snowpack characterizations. *Geophys. Res. Lett.*, **36**, L02503, doi:10.1029/2008GL035214.

Dutra, E., G. Balsamo, P. Viterbo, P. M. A. Miranda, A. Beljaars, C. Schär, and K. Elder, 2010: An improved snow scheme for the ECMWF land surface model: Description and offline validation. *J. Hydrometeor.*, **11**, 899–916, doi:10.1175/2010JHM1249.1.

——, S. Kotlarski, P. Viterbo, G. Balsamo, P. M. A. Miranda, C. Schär, P. Bissolli, and T. Jonas, 2011: Snow cover sensitivity to horizontal resolution, parameterizations, and atmospheric forcing in a land surface model. *J. Geophys. Res.*, **116**, D21109, doi:10.1029/2011JD016061.

Ek, M. B., K. E. Mitchell, Y. Lin, E. Rogers, P. Grunmann, V. Koren, G. Gayno, and J. D. Tarpley, 2003: Implementation of Noah land surface model advances in the National Centers for Environmental Prediction operational mesoscale Eta model. *J. Geophys. Res.*, **108**, 8851, doi:10.1029/2002JD003296.

Essery, R., and Coauthors, 2009: SNOWMIP2: An evaluation of forest snow process simulations. *Bull. Amer. Meteor. Soc.*, **90**, 1120–1135, doi:10.1175/2009BAMS2629.1.

Etchevers, P., and Coauthors, 2004: Validation of the energy budget of an alpine snowpack simulated by several snow models (SnowMIP project). *Ann. Glaciol.*, **38**, 150–158, doi:10.3189/172756404781814825.

Famiglietti, J. S., and Coauthors, 2011: Satellites measure recent rates of groundwater depletion in California's Central Valley. *Geophys. Res. Lett.*, **38**, L03403, doi:10.1029/2010GL046442.

Fassnacht, S. R., K. A. Dressler, and R. C. Bales, 2003: Snow water equivalent interpolation for the Colorado River Basin from snow telemetry (SNOTEL) data. *Water Resour. Res.*, **39**, 1208, doi:10.1029/2002WR001512.

Girotto, M., S. A. Margulis, and M. Durand, 2014: Probabilistic SWE reanalysis as a generalization of deterministic SWE reconstruction techniques. *Hydrol. Processes*, **28**, 3875–3895, doi:10.1002/hyp.9887.

Guan, B., N. P. Molotch, D. E. Waliser, S. M. Jepsen, T. H. Painter, and J. Dozier, 2013: Snow water equivalent in the Sierra Nevada: Blending snow sensor observations with snowmelt model simulations. *Water Resour. Res.*, **49**, 5029–5046, doi:10.1002/wrcr.20387.

Hayhoe, K., and Coauthors, 2004: Emissions pathways, climate change, and impacts on California. *Proc. Natl. Acad. Sci. USA*, **101**, 12 422–12 427, doi:10.1073/pnas.0404500101.

Hedrick, A., H.-P. Marshall, A. Winstral, K. Elder, S. Yueh, and D. Cline, 2015: Independent evaluation of the SNODAS snow depth product using regional-scale lidar-derived measurements. *Cryosphere*, **9**, 13–23, doi:10.5194/tc-9-13-2015.

Hong, S.-Y., Y. Noh, and J. Dudhia, 2006: A new vertical diffusion package with an explicit treatment of entrainment processes. *Mon. Wea. Rev.*, **134**, 2318–2341, doi:10.1175/MWR3199.1.

Howat, I. M., and S. Tulaczyk, 2005: Climate sensitivity of spring snowpack in the Sierra Nevada. *J. Geophys. Res.*, **110**, F04021, doi:10.1029/2005JF000356.

Ikeda, K., and Coauthors, 2010: Simulation of seasonal snowfall over Colorado. *Atmos. Res.*, **97**, 462–477, doi:10.1016/j.atmosres.2010.04.010.

IPCC, 2013: *Climate Change 2013: The Physical Science Basis*. Cambridge University Press, 1535 pp., doi:10.1017/CBO9781107415324.

Jin, J., and N. L. Miller, 2011: Improvement of snowpack simulations in a regional climate model. *Hydrol. Processes*, **25**, 2202–2210, doi:10.1002/hyp.7975.

Jordan, R., 1991: A one-dimensional temperature model for a snow cover: Technical documentation for SNTHERM.89. Special Rep. 91-16, Cold Region Research and Engineers Laboratory, U.S. Army Corps of Engineers, Hanover, NH, 61 pp.

Kain, J. S., 2004: The Kain–Fritsch convective parameterization: An update. *J. Appl. Meteor.*, **43**, 170–181, doi:10.1175/1520-0450(2004)043<0170:TKCPAU>2.0.CO;2.

——, and J. M. Fritsch, 1990: A one-dimensional entraining/detraining plume model and its application in convective parameterization. *J. Atmos. Sci.*, **47**, 2784–2802, doi:10.1175/1520-0469(1990)047<2784:AODEPM>2.0.CO;2.

——, and ——, 1993: Convective parameterization for mesoscale models: The Kain–Fritsch scheme. *The Representation of Cumulus Convection in Numerical Models*, *Meteor. Monogr.*, No. 24, Amer. Meteor. Soc., 165–170.

Kalnay, E., and Coauthors, 1996: The NCEP/NCAR 40-Year Reanalysis Project. *Bull. Amer. Meteor. Soc.*, **77**, 437–471, doi:10.1175/1520-0477(1996)077<0437:TNYRP>2.0.CO;2.

Kapnick, S., and A. Hall, 2010: Observed climate–snowpack relationships in California and their implications for the future. *J. Climate*, **23**, 3446–3456, doi:10.1175/2010JCLI2903.1.

——, and T. L. Delworth, 2013: Controls of global snow under a changed climate. *J. Climate*, **26**, 5537–5562, doi:10.1175/JCLI-D-12-00528.1.

Keighton, S., and Coauthors, 2009: A collaborative approach to study northwest flow snow in the Southern Appalachians. *Bull. Amer. Meteor. Soc.*, **90**, 979–991, doi:10.1175/2009BAMS2591.1.

Kienzle, S. W., 2008: A new temperature based method to separate rain and snow. *Hydrol. Processes*, **22**, 5067–5085, doi:10.1002/hyp.7131.

Koster, R. D., and M. J. Suarez, 1994: The components of a SVAT scheme and their effects on a GCM's hydrological cycle. *Adv. Water Resour.*, **17**, 61–78, doi:10.1016/0309-1708(94)90024-8.

——, and ——, 1996: Energy and water balance calculations in the Mosaic LSM. NASA Tech. Memo. 104606, Vol. 9, 60 pp. [Available online at http://gmao.gsfc.nasa.gov/pubs/docs/Koster130.pdf.]

Lettenmaier, D. P., D. Alsdorf, J. Dozier, G. J. Huffman, M. Pan, and E. F. Wood, 2015: Inroads of remote sensing into hydrologic science during the WRR era. *Water Resour. Res.*, **51**, 7309–7342, doi:10.1002/2015WR017616.

Leung, L. R., and Y. Qian, 2003: The sensitivity of precipitation and snowpack simulations to model resolution via nesting in regions of complex terrain. *J. Hydrometeor.*, **4**, 1025–1043, doi:10.1175/1525-7541(2003)004<1025:TSOPAS>2.0.CO;2.

Liang, X., D. P. Lettenmaier, E. F. Wood, and S. J. Burges, 1994: A simple hydrologically based model of land surface water and energy fluxes for general circulation models. *J. Geophys. Res.*, **99**, 14 415–14 428, doi:10.1029/94JD00483.

Livneh, B., Y. Xia, K. E. Mitchell, M. B. Ek, and D. P. Lettenmaier, 2010: Noah LSM snow model diagnostics and enhancements. *J. Hydrometeor.*, **11**, 721–738, doi:10.1175/2009JHM1174.1.

Lo, J. C.-F., Z.-L. Yang, and R. A. Pielke Sr., 2008: Assessment of three dynamical climate downscaling methods using the Weather Research and Forecasting (WRF) Model. *J. Geophys. Res.*, **113**, D09112, doi:10.1029/2007JD009216.

Lundquist, J. D., P. J. Neiman, B. Martner, A. B. White, D. J. Gottas, and F. M. Ralph, 2008: Rain versus snow in the Sierra Nevada, California: Comparing Doppler profiling radar and surface observations of melting level. *J. Hydrometeor.*, **9**, 194–211, doi:10.1175/2007JHM853.1.

——, S. E. Dickerson-Lange, J. A. Lutz, and N. C. Cristea, 2013: Lower forest density enhances snow retention in regions with warmer winters: A global framework developed from plot-scale observations and modeling. *Water Resour. Res.*, **49**, 6356–6370, doi:10.1002/wrcr.20504.

——, M. Hughes, B. Henn, E. D. Gutmann, B. Livneh, J. Dozier, and P. Neiman, 2015: High-elevation precipitation patterns: Using snow measurements to assess daily gridded datasets across the Sierra Nevada, California. *J. Hydrometeor.*, **16**, 1773–1792, doi:10.1175/JHM-D-15-0019.1.

Mankin, J. S., D. Viviroli, D. Singh, A. Y. Hoekstra, and N. S. Diffenbaugh, 2015: The potential for snow to supply human water demand in the present and future. *Environ. Res. Lett.*, **10**, 114016, doi:10.1088/1748-9326/10/11/114016.

Margulis, S. A., G. Cortés, M. Girotto, and M. Durand, 2016: A Landsat-era Sierra Nevada (USA) snow reanalysis (1985–2015). *J. Hydrometeor.*, **17**, 1203–1221, doi:10.1175/JHM-D-15-0177.1.

Marks, D., A. Winstral, M. Reba, J. Pomeroy, and M. Kumar, 2013: An evaluation of methods for determining during-storm precipitation phase and the rain/snow transition elevation at the surface in a mountain basin. *Adv. Water Resour.*, **55**, 98–110, doi:10.1016/j.advwatres.2012.11.012.

Maussion, F., D. Scherer, R. Finkelnburg, J. Richters, W. Yang, and T. Yao, 2011: WRF simulation of a precipitation event over the Tibetan Plateau, China—An assessment using remote sensing and ground observations. *Hydrol. Earth Syst. Sci.*, **15**, 1795–1817, doi:10.5194/hess-15-1795-2011.

Meng, J., R. Yang, H. Wei, M. Ek, G. Gayno, P. Xie, and K. Mitchell, 2012: The land surface analysis in the NCEP Climate Forecast System Reanalysis. *J. Hydrometeor.*, **13**, 1621–1630, doi:10.1175/JHM-D-11-090.1.

Meromy, L., N. P. Molotch, T. E. Link, S. R. Fassnacht, and R. Rice, 2013: Subgrid variability of snow water equivalent at operational snow stations in the western USA. *Hydrol. Processes*, **27**, 2383–2400, doi:10.1002/hyp.9355.

Mesinger, F., and Coauthors, 2006: North American Regional Reanalysis. *Bull. Amer. Meteor. Soc.*, **87**, 343–360, doi:10.1175/BAMS-87-3-343.

Meybeck, M., P. Green, and C. Vörösmarty, 2001: A new typology for mountains and other relief classes. *Mt. Res. Dev.*, **21**, 34–45, doi:10.1659/0276-4741(2001)021[0034:ANTFMA]2.0.CO;2.

Minder, J. R., P. W. Mote, and J. D. Lundquist, 2010: Surface temperature lapse rates over complex terrain: Lessons from the Cascade Mountains. *J. Geophys. Res.*, **115**, D14122, doi:10.1029/2009JD013493.

Mitchell, K. E., and Coauthors, 2004: The multi-institution North American Land Data Assimilation System (NLDAS): Utilizing multiple GCIP products and partners in a continental distributed hydrological modeling system. *J. Geophys. Res.*, **109**, D07S90, doi:10.1029/2003JD003823.

Mlawer, E. J., S. J. Taubman, P. D. Brown, M. J. Iacono, and S. A. Clough, 1997: Radiative transfer for inhomogeneous atmospheres: RRTM, a validated correlated-*k* model for the longwave. *J. Geophys. Res.*, **102**, 16 663–16 682, doi:10.1029/97JD00237.

Molotch, N. P., and R. C. Bales, 2005: Scaling snow observations from the point to the grid element: Implications for observation network design. *Water Resour. Res.*, **41**, W11421, doi:10.1029/2005WR004229.

Mudryk, L. R., C. Derksen, P. J. Kushner, and R. Brown, 2015: Characterization of Northern Hemisphere snow water equivalent datasets, 1981–2010. *J. Climate*, **28**, 8037–8051, doi:10.1175/JCLI-D-15-0229.1.

National Operational Hydrologic Remote Sensing Center, 2004: Snow Data Assimilation System (SNODAS) data products at NSIDC, version 1. National Snow and Ice Data Center, accessed 6 January 2017, doi:10.7265/N5TB14TC.

Niu, G. Y., and Coauthors, 2011: The community Noah land surface model with multiparameterization options (Noah-MP): 1. Model description and evaluation with local-scale measurements. *J. Geophys. Res.*, **116**, D12109, doi:10.1029/2010JD015139.

Nolin, A. W., 2012: Perspectives on climate change, mountain hydrology, and water resources in the Oregon Cascades, USA. *Mt. Res. Dev.*, **32**, S35–S46, doi:10.1659/MRD-JOURNAL-D-11-00038.S1.

Pan, M., and Coauthors, 2003: Snow process modeling in the North American Land Data Assimilation System (NLDAS): 2. Evaluation of model simulated snow water equivalent. *J. Geophys. Res.*, **108**, 8850, doi:10.1029/2003JD003994.

Pavelsky, T. M., S. Kapnick, and A. Hall, 2011: Accumulation and melt dynamics of snowpack from a multiresolution regional climate model in the central Sierra Nevada, California. *J. Geophys. Res.*, **116**, D16115, doi:10.1029/2010JD015479.

——, S. Sobolowsk, S. B. Kapnick, and J. B. Barnes, 2012: Changes in orographic precipitation patterns caused by a shift from snow to rain. *Geophys. Res. Lett.*, **39**, L18706, doi:10.1029/2012GL052741.

Pepin, N. C., and Coauthors, 2015: Elevation-dependent warming in mountain regions of the world. *Nat. Climate Change*, **5**, 424–430, doi:10.1038/nclimate2563.

Rasmussen, R., and Coauthors, 2011: High-resolution coupled climate runoff simulations of seasonal snowfall over Colorado: A process study of current and warmer climate. *J. Climate*, **24**, 3015–3048, doi:10.1175/2010JCLI3985.1.

Reichle, R. H., R. D. Koster, G. J. M. De Lannoy, B. A. Forman, Q. Liu, S. P. P. Mahanama, and A. Touré, 2011: Assessment and enhancement of MERRA land surface hydrology estimates. *J. Climate*, **24**, 6322–6338, doi:10.1175/JCLI-D-10-05033.1.

Renwick, J., 2014: MOUNTerrain: GEWEX mountainous terrain precipitation project. *GEWEX News*, Vol. 24, No. 4, International GEWEX Project Office, Silver Spring, MD, 5–6. [Available online at http://www.gewex.org/gewex-content/files_mf/1432213914Nov2014.pdf.]

Rienecker, M. M., and Coauthors, 2011: MERRA: NASA's Modern-Era Retrospective Analysis for Research and Applications. *J. Climate*, **24**, 3624–3648, doi:10.1175/JCLI-D-11-00015.1.

Rodell, M., and Coauthors, 2004: The Global Land Data Assimilation System. *Bull. Amer. Meteor. Soc.*, **85**, 381–394, doi:10.1175/BAMS-85-3-381.

Rutter, N., and Coauthors, 2009: Evaluation of forest snow processes models (SnowMIP2). *J. Geophys. Res.*, **114**, D06111, doi:10.1029/2008JD011063.

Salzmann, N., and L. O. Mearns, 2012: Assessing the performance of multiple regional climate model simulations for seasonal mountain snow in the Upper Colorado River Basin. *J. Hydrometeor.*, **13**, 539–556, doi:10.1175/2011JHM1371.1.

Schmidt, R., and Coauthors, 2006: GRACE observations of changes in continental water storage. *Global Planet. Change*, **50**, 112–126, doi:10.1016/j.gloplacha.2004.11.018.

Shamir, E., and K. P. Georgakakos, 2006: Distributed snow accumulation and ablation modeling in the American River basin. *Adv. Water Resour.*, **29**, 558–570, doi:10.1016/j.advwatres.2005.06.010.

Sheffield, J., and Coauthors, 2003: Snow process modeling in the North American Land Data Assimilation System (NLDAS): 2. Evaluation of model simulated snow water equivalent. *J. Geophys. Res.*, **108**, 8849, doi:10.1029/2002JD003274.

Skamarock, W. C., and Coauthors, 2008: A description of the Advanced Research WRF version 3. NCAR Tech. Note NCAR/TN-475+STR, 113 pp., doi:10.5065/D68S4MVH.

Snauffer, A. M., W. W. Hsieh, and A. J. Cannon, 2016: Comparison of gridded snow water equivalent products with in situ measurements in British Columbia, Canada. *J. Hydrol.*, **541**, 714–726, doi:10.1016/j.jhydrol.2016.07.027.

Sturm, M., J. Holmgren, and G. E. Liston, 1995: A seasonal snow cover classification system for local to global applications. *J. Climate*, **8**, 1261–1283, doi:10.1175/1520-0442(1995)008<1261:ASSCCS>2.0.CO;2.

Sultana, R., K.-L. Hsu, J. Li, and S. Sorooshian, 2014: Evaluating the Utah Energy Balance (UEB) snow model in the Noah land-surface model. *Hydrol. Earth Syst. Sci.*, **18**, 3553–3570, doi:10.5194/hess-18-3553-2014.

Syed, T. H., J. S. Famiglietti, M. Rodell, J. Chen, and C. R. Wilson, 2008: Analysis of terrestrial water storage changes from GRACE and GLDAS. *Water Resour. Res.*, **44**, W02433, doi:10.1029/2006WR005779.

Takala, M., K. Luojus, J. Pulliainen, C. Derksen, J. Lemmetyinen, J. P. Kärnä, J. Koskinen, and B. Bojkov, 2011: Estimating northern hemisphere snow water equivalent for climate research through assimilation of space-borne radiometer data and ground-based measurements. *Remote Sens. Environ.*, **115**, 3517–3529, doi:10.1016/j.rse.2011.08.014.

Tedesco, M., and P. S. Narvekar, 2010: Assessment of the NASA AMSR-E SWE product. *IEEE J. Sel. Top. Appl. Earth Obs. Remote Sens.*, **3**, 141–159, doi:10.1109/JSTARS.2010.2040462.

——, R. Kelly, J. L. Foster, and A. T. C. Chang, 2004: AMSR-E/*Aqua* Daily L3 Global Snow Water Equivalent EASE-Grids, version 2. Subset used: 2002 to present (updated daily). NASA National Snow and Ice Data Center Distributed Active Archive Center, accessed 6 January 2017, doi:10.5067/AMSR-E/AE_DYSNO.002.

Thompson, G., R. M. Rasmussen, and K. Manning, 2004: Explicit forecasts of winter precipitation using an improved bulk microphysics scheme. Part I: Description and sensitivity analysis. *Mon. Wea. Rev.*, **132**, 519–542, doi:10.1175/1520-0493(2004)132<0519:EFOWPU>2.0.CO;2.

Verseghy, D. L., 1991: CLASS—A Canadian Land Surface Scheme for GCMS. I. Soil model. *Int. J. Climatol.*, **11**, 111–133, doi:10.1002/joc.3370110202.

Viviroli, D., H. H. Dürr, B. Messerli, M. Meybeck, and R. Weingartner, 2007: Mountains of the world, water towers for humanity: Typology, mapping, and global significance. *Water Resour. Res.*, **43**, W07447, doi:10.1029/2006WR005653.

Vuyovich, C. M., C. V. Henri, and D. Fern, 2014: Comparison of passive microwave and modeled estimates of total watershed SWE in the continental United States. *Water Resour. Res. Res.*, **50**, 9088–9102, doi:10.1002/2013WR014734.

Waliser, D., and Coauthors, 2011: Simulating the Sierra Nevada snowpack: The impact of snow albedo and multi-layer snow physics. *Climatic Change*, **109**, 95–117, doi:10.1007/s10584-011-0312-5.

Wei, H., Y. Xia, K. E. Mitchell, and M. B. Ek, 2013: Improvement of the Noah land surface model for warm season processes: Evaluation of water and energy flux simulation. *Hydrol. Processes*, **27**, 297–303, doi:10.1002/hyp.9214.

Wood, E. F., D. Lettenmaier, X. Liang, B. Nijssen, and S. W. Wetzel, 1997: Hydrological modeling of continental-scale basins. *Annu. Rev. Earth Planet. Sci.*, **25**, 279–300, doi:10.1146/annurev.earth.25.1.279.

Wrzesien, M. L., T. M. Pavelsky, S. B. Kapnick, M. T. Durand, and T. H. Painter, 2015: Evaluation of snow cover fraction for regional climate simulations in the Sierra Nevada. *Int. J. Climatol.*, **35**, 2472–2484, doi:10.1002/joc.4136.

Xia, Y., and Coauthors, 2012a: Continental-scale water and energy flux analysis and validation for North American Land Data Assimilation System project phase 2 (NLDAS-2): 1. Intercomparison and application of model products. *J. Geophys. Res.*, **117**, D03109, doi:10.1029/2011JD016048.

——, and Coauthors, 2012b: Continental-scale water and energy flux analysis and validation for North American Land Data Assimilation System project phase 2 (NLDAS-2): 2. Validation of model-simulated streamflow. *J. Geophys. Res.*, **117**, D03110, doi:10.1029/2011JD016051.

Xu, L., and P. Dirmeyer, 2011: Snow–atmosphere coupling strength in a global atmospheric model. *Geophys. Res. Lett.*, **38**, L13401, doi:10.1029/2011GL048049.